NUCL SCI TECH (2016) 27:46
DOI 10.1007/s41365-016-0047-0

Performance comparison of the two ICRF antennas in EAST

Hua Yang[1] · Cong-Feng Wu[1] · Sai Dong[1] · Yan-Ping Zhao[2] · Xin-Jun Zhang[2] · Lei Shang[1]

Received: 10 March 2015 / Revised: 2 August 2015 / Accepted: 31 August 2015 / Published online: 12 April 2016

Abstract The experimental advanced superconducting Tokamak has two suits of ion cyclotron radio frequency heating systems, in which the two antennas are of different structures. Their performance is assessed and compared by CST microwave studio. The radiating capacity of antennas and the arcing around them are estimated. The impurity release is analyzed by the radio frequency (RF) potential in the plasma sheath. The simulation results show that the radiating capacity for the folded antenna (I-port) is better than those for the double loops antenna (B-port). However, the folded antenna is worse than the double loops antenna in terms of breakdown. Moreover, the impurity production is relevant to spectrum shaping. The RF potential at (0, π, π, 0) phasing with the peak of spectrum $k_{//} = 8.5\ \mathrm{m}^{-1}$ is lower than the one with other phases. The impurity is reduced obviously when the folded antenna is powered with (0, π, π, 0) phasing.

Keywords ICRF antenna · EAST · Arcing · Impurity

1 Introduction

The experimental advanced superconducting Tokamak (EAST) is an advanced steady-state plasma experimental device. Ion cyclotron resonance heating (ICRH), an important heating method for a fusion reactor due to a direct ion heating at high density, is a reliable technology for high power handling and low cost. EAST has two ICRF antenna systems, powered each by 6 MW continuous wave. With a frequency range of 25–70 MHz, the ICRF systems in the EAST may provide plasma heating and current drive under various scenarios over a range of magnetic fields [1].

In the 2012 experimental campaign, the high-confinement (H-mode) discharges were obtained by ICRF heating alone [2]. The H-mode plasmas were produced at plasma currents of 0.4–0.6 MA, line-averaged density of $(1.83–2.35) \times 10^{19}\ \mathrm{m}^{-3}$, and $B_0 = 1.85–1.95$ T. The power for ICRF antenna varied from 1.6 to 1.8 MW.

Two antennas based on different design proposals were developed and fabricated. Antenna 1, at B-port (2-straps), is grounded at the center and has a coaxial feed line connected to each end of the current strap. Antenna 2, at I-port, has four current straps. The antenna straps are end-grounded center-fed folded design. At present, a great amount of ICRF antennas have adopted the similar structure as the two antennas in EAST. For example, the Alcator C-Mod [3] has two ICRF antennas similar to the two antennas in EAST; the ITER-like ICRF antenna in JET [4] and the antenna in Tore–Supra [5] are the same as the antenna at B-port in EAST. The ICRF antenna in ASDEX upgrade [6] has the structure like the antenna at I-port in EAST.

Mechanical analysis of the two antennas and the reference design of 2-strap antenna in EAST have been done

Supported by the National Magnetic Confinement Fusion Science Program of China (No. 2015GB101001) and the Natural Science Foundation of China (No. 11375236).

✉ Cong-Feng Wu
cfwu@ustc.edu.cn

[1] National Synchrotron Radiation Laboratory, University of Science and Technology of China, Hefei 230029, China

[2] Institute of Plasma Physics, Chinese Academy of Sciences, Hefei 230031, China

[7–9]. To the author's knowledge, there is little information available in the literature about the comparison of the two ICRF antenna types. In recent years, several 3D electromagnetic codes have been used to analyze and optimize the ICRF antenna. The 3D CST microwave studio (MWS) code was used for the ICRF antenna in JET [10] and ITER [11]. The motivation behind this work is to compare the performance of the two types of ICRF antenna in EAST and provides references for future ICRF antenna design. Performance of an antenna is mainly limited by arcing and impurities [3]. In this paper, we will concentrate on the breakdown and impurity release of the two antennas in EAST.

2 Simulation on ICRF antennas in EAST

Antenna 1 is installed at B-port with two toroidal straps and is grounded at the center and connected to each end of the current strap with a coaxial feed line (Fig. 1a), while Antenna 2 is installed at I-port with four current straps of end-grounded center-fed folded design (Fig. 1b). It is noted that the Faraday screens are not fully shown here. Four 1.5 MW RF transmitters are powered to each antenna. The 4-strap antenna design adds the capacity of a directly launched wave spectrum for current drive through the changes in current strap phasing. Each antenna unit includes the straps, Faraday screens, box and coaxial lines. The rod of Faraday screen with the radius of 10 mm is in front of the surface of strap by 10 mm.

Performance of the antennas was analyzed by CST MWS, a 3D electromagnetic code. The plasma was simulated by a slab of dielectric with a high relative permittivity. The models of the straps are shown in Fig. 2. The plasma is 50 mm in front of straps and 30 mm away from the surface of Faraday screens. Straps of the B-port and I-port antennas are of the same length (760 mm) and width (100 mm).

3 Results and discussion

3.1 Radiating capacity

In general, the radiating capacity of RF or microwave antenna is mainly assessed by scattering parameter and lobe pattern. However, the plasma is located in the near-field place, where there is more than one feed port. The scattering parameters at one port of the antennas are shown in Fig. 3. The mutual coupling is strong between the straps, especially the S21 in double loops antenna (Fig. 3a). So the scattering parameter is importance, but is not perfectly adequate for reflecting the radio capacity of antenna integral. The return loss for estimating the radio capacity at all ports is defined as [12]:

$$\mathrm{RL} = 10\log(P_{\mathrm{in}}/P_{\mathrm{out}}),$$

where P_{out} is the backward power from antenna and P_{in} is the forward power. The higher the RL is, the better the power is radiated by antenna.

The RL of two antennas is shown in Fig. 3c. The RL of Antenna 1 is lower than the RL of Antenna 2. It is mean that the Antenna 2 has a better radiating capacity under the same size as Antenna 1. Though the S_{11} of the Antenna 1 is better, the mutual coupling of straps in Antenna 1 is larger.

3.2 Breakdown around antenna

In current ICRF systems, the antenna performance is severely limited by the breakdown and arcing. A high voltage arc is affected by the pressure, frequency and material and so on. Besides, the influence of ions on the high voltage arc of ICRF antenna is important. Ion bombardment of the metal makes the secondary electron emission which may be accelerated by a high E-field. If the E-field is high enough, the arcing is easy to occur in the high E-field area.

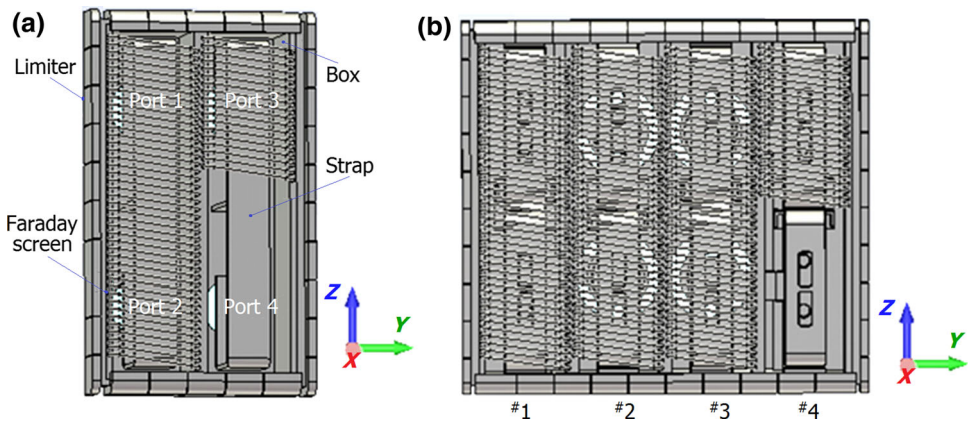

Fig. 1 Antenna 1 at B-port (**a**) and Antenna 2 at I-port (**b**), in EAST

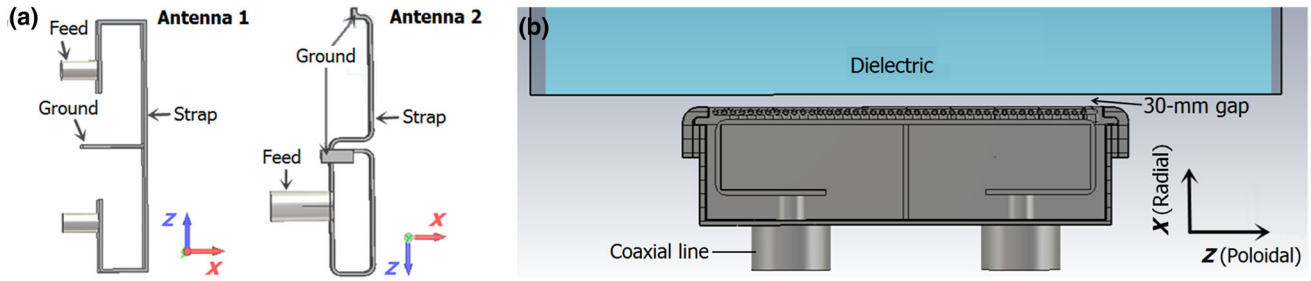

Fig. 2 The antenna strap structures (**a**) and antenna model of typical distance between the Faraday screens and plasma in CST MWS (**b**)

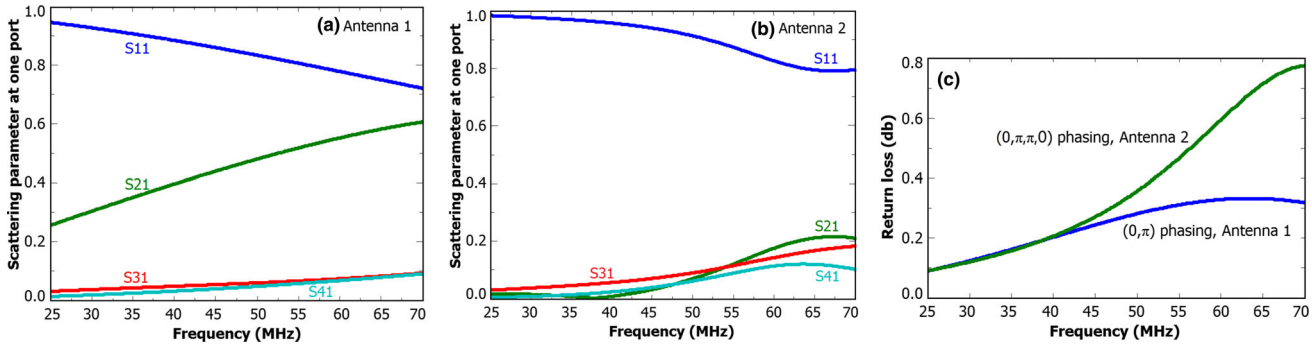

Fig. 3 The scattering parameter at one port of Antennas 1 (**a**) and 2 (**b**) and the return loss of the antennas

Empirical data were obtained in Alcator C-mod [3]. For the structure around the antenna and box, the breakdown voltage is allowed to reach about 35 kV/cm for the RF E-field across the B-field and is about 15 kV/cm for $E||B$. It is noted that the breakdown voltage is related to their location just as the limited voltage is 45 kV in the transmission line. For the Alcator C-Mod antenna, the breakdown occurred in the feed strap line connecting the coaxial line and current strap [13]. In EAST, arcing caused by increasing backward RF power has been observed.

The maxima of E-field around Antenna 1 of (0, π) and (0, $\pi/2$) phasing are calculated at 18.45 and 21.18 kV/cm, respectively; and the maxima of E-field around Antenna 2 of (0, 0, π, π), (0, $\pi/2$, π, $3\pi/2$) and (0, π, π, 0) phasing are calculated at 32.82, 30.20 and 27.54 kV/cm, respectively. The working frequency of antennas is 55 MHz. The E_{max} at the (0, π) phasing for Antenna 1 is lower than that at the (0, $\pi/2$) phasing, while for Antenna 2, the E_{max} at the (0, π, π, 0) phasing is lower than those at other phases. It can also be seen that the structure of Antenna 1 is appropriate for decreasing the high E-field. E_{max} of Antenna 1 at (0, π) phasing is only 2/3 of E_{max} of Antenna 2 at (0, π, π, 0) phasing.

3.3 Impurity production using ICRF heating

For a Tokamak, an important problem associated with ICRF heating is the increased impurity release. An interpretation of this phenomenon is that the application of ICRF power leads to an appearance of the rectified plasma sheath potential [6]. During ICRF antenna operation, an oscillating RF potential along the total B-field ($E_{//}$) is driven in front of the antenna. Electrons and ions are both accelerated in the RF potential, but the electron move faster than the ion. Electrons are preferentially lost to the conducting surfaces around the ICRF antenna, leading to a rectified potential in the scrape-off layer. Sputtering of the structures and the vessel wall by hydrogen ions and impurity ions accelerated in the sheath potentials is the main cause of the impurity release.

In previous experiments at EAST, increased radiation of metallic impurities was observed and RF sheath-related plasma potential was modified during an RF pulse. The RF potential in front of the antenna was studied at 55 MHz with 4 × 1.5 MW power. Figure 4 shows distributions of the E-field along the B-field at 35 mm in front of the straps. There are the distribution of the $E_{//}$ with (0, π) phasing for Antenna 1 and (0, 0, π, π) phasing for Antenna 2. The location of high $E_{//}$ is mainly close to the limiter and antenna box. The effect of current phasing on the RF potential was investigated with the two antennas. Figure 5 shows the RF potential along the poloidal coordinate. For Antenna 1, the $E_{//}$ fields at (0, π) phasing are higher than those at (0, $\pi/2$) phasing, while for Antenna 2, the $E_{//}$ fields at (0, 0, π, π) phasing are worse than those at the other phases, and the $E_{//}$ fields at (0, π, π, 0) phasing are the lowest.

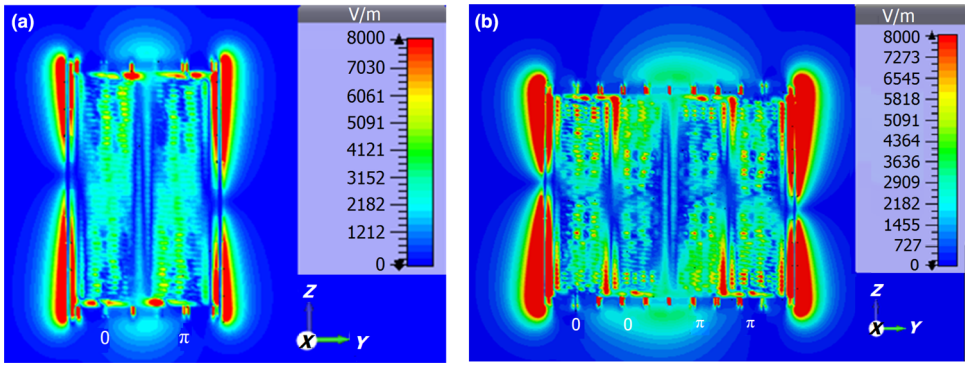

Fig. 4 The distribution of $E_{//}$ at 35 mm in front of Antennas 1 (**a**) and 2 (**b**)

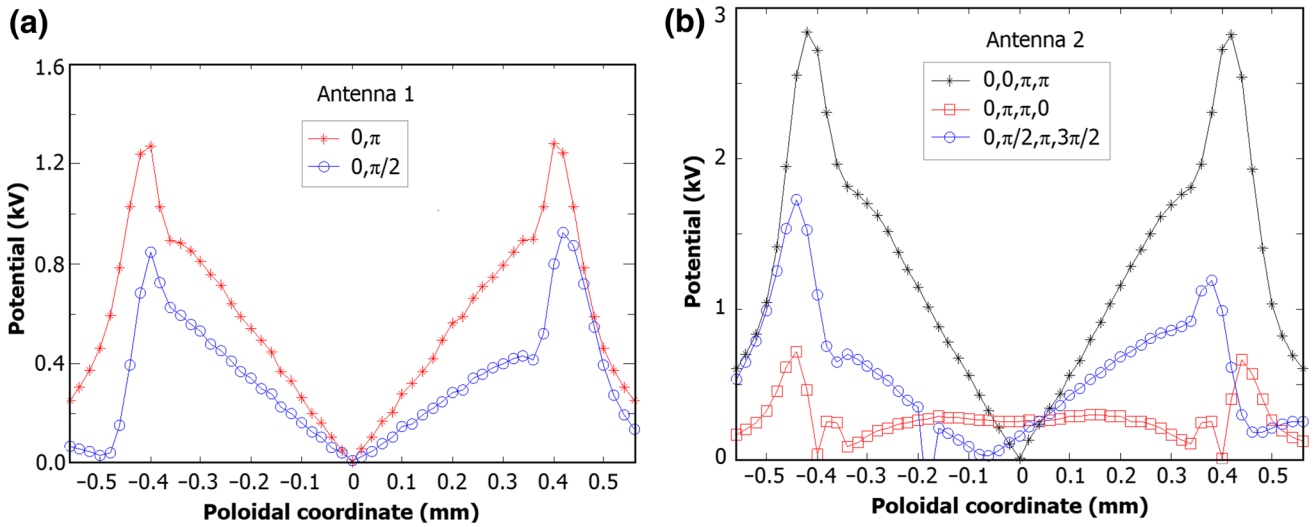

Fig. 5 The RF potential 35 mm in front of the two antennas as function of poloidal position

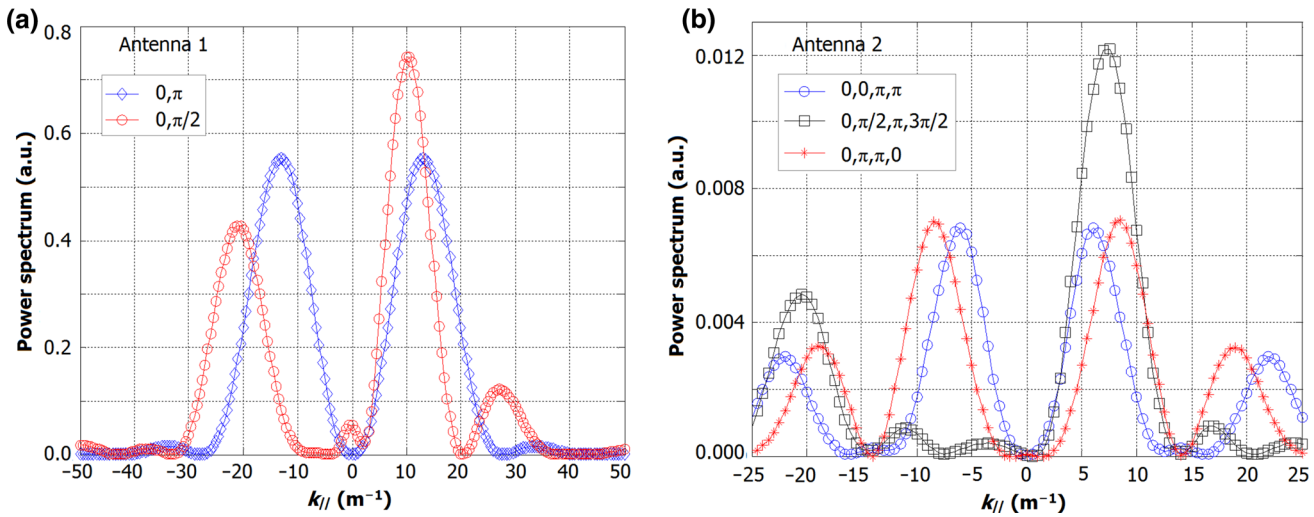

Fig. 6 The antenna spectra as function of $k_{//}$

On the other hand, the impurity production associated with spectrum was studied in many Tokamaks. It was found that the rate of oxygen production at the onset of RF pulse decreased when the $k_{//} = 0$ was not excited in TFR [14]. An obvious reduction of the radiated power during the RF heating was observed in JFT-2M Tokamak [15] when

Table 1 A comparison of the performance of the two ICRF antennas

Performance	Antenna 1 (B-port)	Antenna 2 (I-port)
Radiating capacity	Lower	Higher
Mutual coupling	Higher	Lower
Breakdown and arcing	Better, in (0, π) phasing	Worse
Impurity release	Worse	Better in (0, π, π, 0) phasing

the peak of excited $k_{//}$ spectrum was approximately at 8 m^{-1}. A large amount of metallic ions observed in the plasma during RF were much lower at (0, π, 0, π) phasing of the antennas, with the launched spectrum peaked at $k_{//} = 7$ m^{-1} in JET [4].

The power spectra were calculated for exploring impurity production to the spectrum. The spectra in various phases are shown in Fig. 6. The spectra in (0, π/2) phasing for Antenna 1 and (0, π/2, π, 3π/2) phasing for Antenna 2 are asymmetric. The spectra under the other conditions are symmetric. Besides, the spectrum peaks are 13 m^{-1} in (0, π) phasing and 10.5 m^{-1} in (0, π/2) phasing for Antenna 1, while the peaks in (0, 0, π, π), (0, π, π, 0) and (0, π/2, π, 3π/2) phasings for Antenna 2 are 6, 8.5 and 7.5 m^{-1}, respectively. Above all, the RF potential at (0, π, π, 0) phasing and the spectrum peak of 8.5 m^{-1} is the lowest. The simulation results agree with the experiment results in TFR, JFT-2 M and JET [4, 14, 15].

4 Conclusion

Performance of the two antennas in EAST is analyzed and compared. The radiating capacity, breakdown and the spectrum effects on impurity production are investigated. The 4-strap antenna (I-port) has a better function at radiation power and the mutual coupling of straps than the 2-strap antenna (B-port). The maximum E-field around antenna for the 2-strap antenna at (0, π) phasing is only 2/3 times of the maximum of the 4-strap antenna at (0, π, π, 0) phasing. Besides, the impurity release by ICRF heating is related to $k_{//}$ shaping. The RF potential at (0, π, π, 0) phasing with the spectrum peak of 8.5 m^{-1} for 4-strap antenna is the lowest of all cases. So the 4-strap antenna can reduce impurity production.

Advantages and disadvantages of the two antennas in terms of radiating capacity, mutual coupling, arcing and impurity release are summarized in Table 1. Antenna 2 is better than the Antenna 1 with respect to radiating capacity, arcing and impurity release, but the E-field of Antenna 2 is higher than Antenna 1 under the same feed power.

The arcing of Antenna 2 and impurities release by both antennas have been observed. The antenna performance will be checked in future experiments at EAST. This study provides a reference for upgrade of the ICRF antennas.

Acknowledgments The authors wish to thank Dr. Cheng-Ming Qin for helpful discussions and the EAST ICRF team for their support.

References

1. Y.P. Zhao, X.J. Zhang, Y.Z. Mao et al., EAST ion cyclotron resonance heating system for long pulse operation. Fusion Eng. Des. **89**, 2642–2646 (2014). doi:10.1016/j.fusengdes.2014.06.017
2. X.J. Zhang, Y.P. Zhao, B.N. Wan et al., First results from H-mode plasmas generated by ICRF heating in the EAST. Nucl. Fusion **53**, 023004 (2013). doi:10.1088/0029-5515/53/2/023004
3. S.J. Wukitch, R.L. Boivin, P.T. Bonoli et al., Investigation of performance limiting phenomena in a variable phase ICRF antenna in Alcator C-Mod. Plasma Phys. Control. Fusion **46**, 1479–1491 (2004). doi:10.1088/0741-3335/46/9/010
4. A. Czarnecka, F. Durodié, A.C.A. Figueiredo et al., Impurity production from the ion cyclotron resonance heating antennas in JET. Plasma Phys. Control. Fusion **54**, 074013 (2012). doi:10.1088/0741-3335/54/7/074013
5. K. Vulliez, G. Bosia, G. Agarici et al., Tore supra ICRH antenna prototype for next step devices. Fusion Eng. Des. **66**, 531–535 (2003). doi:10.1016/S0920-3796(03)00099-1
6. V.V. Bobkov, F. Braun, R. Dux et al., Assessment of compatibility of ICRF antenna operation with full W wall in ASDEX Upgrade. Nucl. Fusion **50**, 035004 (2010). doi:10.1088/0029-5515/50/3/035004
7. Q.X. Yang, Y.T. Song, S.T. Wu et al., Mechanical design and first engineering commissioning of ICRF antenna for EAST. Plasma Sci. Technol. **12**, 488–493 (2010). doi:10.1088/1009-0630/12/4/20
8. Q.X. Yang, Y.T. Song, S.T. Wu et al., Mechanical design of the second ICRF antenna for EAST. Fusion Eng. Des. **87**, 1249–1252 (2012). doi:10.1016/j.fusengdes.2012.02.123
9. C.M. Qin, Y.P. Zhao, H. Okada et al., Reference design of ICRF antenna for EAST. Plasma Sci. Technol. **8**, 358–362 (2006). doi:10.1088/1009-0630/8/3/25
10. P.U. Lamalle, A.M. Messiaen, P. Dumortier et al., Recent developments in ICRF antenna modelling. Nucl. Fusion **46**, 432–443 (2006). doi:10.1088/0029-5515/46/4/004
11. F. Louche, P. Dumortier, A. Messiaen et al., 3D electromagnetic optimization of the front face of the ITER ICRF antenna. Nucl. Fusion **51**, 103002 (2011). doi:10.1088/0029-5515/51/10/103002
12. T.S. Bird, Definition and misuse of return loss. IEEE Antennas Propag. Mag. **51**, 166–167 (2009). doi:10.1109/MAP.2009.5162049
13. G. Schilling, S.J. Wukitch, R.L. Boivin et al., Analysis of 4-strap ICRF antenna performance in Alcator C-Mod, vol 694 (AIP Publishing, 2003), p. 166. doi:10.1063/1.1638020
14. TFR Group, F. Sand, ICRF heating experiments in TFR using a low-field-side antenna. Nucl. Fusion **25**, 1719–1732 (1985)
15. H. Tamai, K. Odajima, H. Matsumoto et al., Impurity reduction during ICRF heating in JFT-2M tokamak. Nucl. Fusion **26**, 365–369 (1986)